ACS OMEGA

Open Access

http://pubs.acs.org/journal/acsodf

Article

Kinetics, Equilibrium, and Thermodynamics for Conjugation of Chitosan with Insulin-Mimetic [*meso*-Tetrakis(4-sulfonatophenyl)porphyrinato]oxovanadate(IV)(4−) in an Aqueous Solution

Chironjit Kumar Shaha, Bithy Sarker, Shurid Kishore Mahalanobish, Md. Sharif Hossain, Subarna Karmaker,* and Tapan Kumar Saha*

Cite This: *ACS Omega* 2023, 8, 41612−41623

Read Online

ACCESS | Metrics & More | Article Recommendations

ABSTRACT: This study investigated the conjugation of chitosan with the insulin-mimetic [*meso*-tetrakis(4-sulfonatophenyl)porphyrinato]-oxovanadate(IV)(4−), VO(tpps), in an aqueous medium as a function of conjugation time, VO(tpps) concentrations, and temperatures. To validate the synthesis of chitosan-VO(tpps) conjugate, UV−visible and Fourier transform infrared spectrophotometric techniques were utilized. Conjugate formation is ascribed to the electrostatic interaction between the NH_3^+ units of chitosan and the SO_3^- units of VO(tpps). Chitosan enhances the stability of VO(tpps) in an aqueous medium (pH 2.5). VO(tpps) conjugation with chitosan was best explained by pseudo-second-order kinetic and Langmuir isotherm models based on kinetic and isotherm studies. The Langmuir equation determined that the maximal ability of VO(tpps) conjugated with each gram of chitosan was 39.22 μmol at a solution temperature of 45 °C. Activation energy and thermodynamic studies (E_a: 8.78 kJ/mol, ΔG: −24.52 to −27.55 kJ/mol, ΔS: 204.22 J/(mol K), and ΔH: 37.30 kJ/mol) reveal that conjugation is endothermic and physical in nature. The discharge of VO(tpps) from conjugate was analyzed in freshly prepared 0.1 mol/L phosphate buffer (pH 7.4) at 37 °C. The release of VO(tpps) from the conjugate is a two-phase process best explained by the Higuchi model, according to a kinetic analysis of the release data. Taking into consideration all experimental findings, it is proposed that chitosan can be used to formulate both solid and liquid insulin-mimetic chitosan-VO(tpps) conjugates.

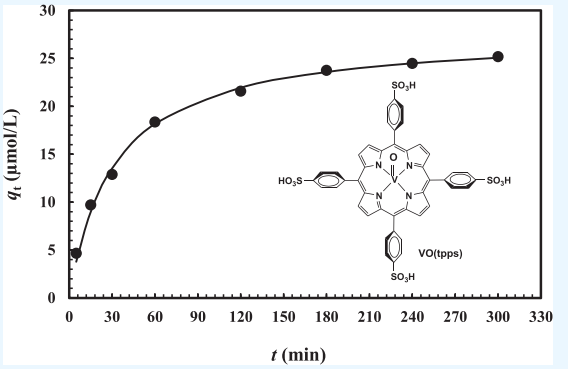

INTRODUCTION

In biotechnology, enzymatic catalysis, medicine, and therapeutics, the conjugation of polymer with bioactive molecules has attracted considerable scientific interest.[1] Intensive research is being conducted to develop polymer-based therapeutic systems.[2,3] Polymer conjugation increases the therapeutics' stability and efficacy.[4] In the formulation of therapeutic agents, various polymers such as poly[*N*-(2-hydroxy-propyl)methacrylamide],[5] polyacrylamide,[6] poly(vinyl alcohol),[7] poly(γ-glutamic acid),[8] and chitosan[9] have been utilized as carriers.

Chitosan (Figure 1a) is a deacetylated product of chitin that occurs naturally as structural building blocks in the shell of insects and fungal cell walls.[10] It is believed that chitosan's unique structure (a high proportion of primary amines) is responsible for its many physicochemical properties.[11] Chitosan's high sorption capacity offers a promising method for removing organic dyes, heavy metals, and pharmaceutical contaminants from effluent water.[12−14] Its positively charged surface facilitates electrostatic interactions with anionic species. Chitosan is a versatile biomolecule[15−17] due to its numerous medicinal properties, including antidiabetic. Due to its high mucoadhesiveness and minimal production cost, chitosan is frequently used as a carrier for oral therapeutics.[18] Chitosan-based therapeutic strategies are regarded as a viable method for managing diabetes.[19−21]

There are multiple applications for naturally occurring porphyrins and their metal complexes in various research disciplines, including dye degradation,[22] sonodynamic anticancer therapy,[23] photodynamic therapy,[24,25] MRI contrast agent,[26] drug delivery,[27] single-cell imaging,[28] and antimicro-

Received: August 7, 2023
Revised: October 7, 2023
Accepted: October 11, 2023
Published: October 24, 2023

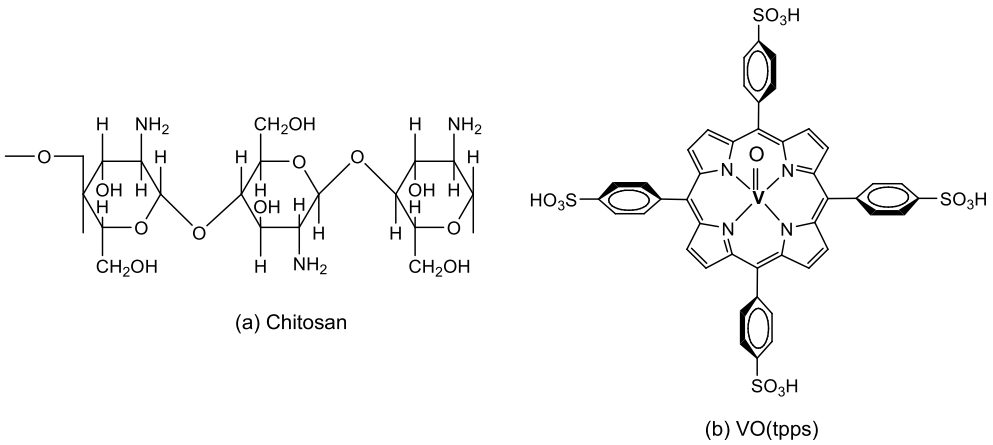

Figure 1. Structure of chitosan (a) and [*meso*-tetrakis(4-sulfonatophenyl)porphyrinato]oxovanadate (IV) (4−), VO(tpps) (b).

bial to cancer treatment.[29−31] VO(tpps) (Figure 1b) is a water-soluble insulin-mimetic vanadyl-porphyrin complex for oral therapy of type 1 and type 2 diabetes mellitus in animals.[32,33] VO(tpps) is regarded as an effective insulin-mimetic complex.

These significant results prompted us to investigate the chitosan-VO(tpps) conjugation mechanism based on kinetics, equilibrium isotherm, and thermodynamics, thus paving the way for chitosan-based metallodrug delivery. In this study, chitosan-VO(tpps) conjugate was synthesized and characterized, and the kinetics and equilibrium of conjugation in aqueous solution were investigated. Particularly, the effects of various conjugation parameters, including conjugation time, VO(tpps) concentration, and solution temperature, were examined. We observed equilibrium conjugation between VO(tpps) and chitosan in an aqueous medium at numerous temperatures. The kinetic and isotherm data obtained from chitosan-VO(tpps) conjugation experiments were evaluated using kinetic (pseudo-first-order, pseudo-second-order, and Elovich), diffusion (film diffusion and intraparticle diffusion), and isotherm (Freundlich, Temkin, and Langmuir) models. In an aqueous environment, the activation and thermodynamic characteristics for the conjugation between VO(tpps) and chitosan were evaluated. We investigated the stability of the chitosan-VO(tpps) conjugate in an acidic medium (pH 2.5). The experiment of VO(tpps) in vitro release from chitosan-VO(tpps) conjugate was conducted in 0.1 mol/L phosphate buffer (pH 7.4) at 37 °C.

RESULTS AND DISCUSSION

Chitosan-VO(tpps) Conjugate Synthesis and Characterization. A straightforward technique was used to conjugate VO(tpps) with chitosan in an aqueous medium without adding any cross-linking agent. Aqueous solution of VO(tpps) (4 μmol/L) was added to chitosan solution (1% w/v; pH 2.5) at 1:1 (v/v) ratio with continuous stirring to facilitate conjugation, which was evaluated by spectroscopically.[34] The UV−vis absorption spectra of chitosan, VO(tpps), and chitosan-VO(tpps) complex in an aqueous medium are exhibited in Figure 2. The characteristic peak of chitosan at 287 nm (Figure 2a) was moved to 295 nm in the complex (Figure 2c). Consequently, the 8 nm bathochromic shift of the chitosan characteristic peak was attributed to conjugate formation in an aqueous environment.[34] In VO(tpps), the soret band appeared at 436 nm (Figure 2b), whereas in the conjugate, it shifted to 413 nm (Figure 2c). Moreover, the Q-band at 564 nm was moved to a higher wavelength (566 nm), and a second Q-band at 603 nm was removed from the conjugate spectrum (Figure 2c). As seen in Figure 2, the significant hypsochromic shift (23 nm) of the soret band and the bathochromic shift (2 nm) of the Q-band indicate the effective conjugation of VO(tpps) and chitosan in an aqueous environment. The chitosan-VO(tpps) complex also exhibited comparable spectral observations.[35−37]

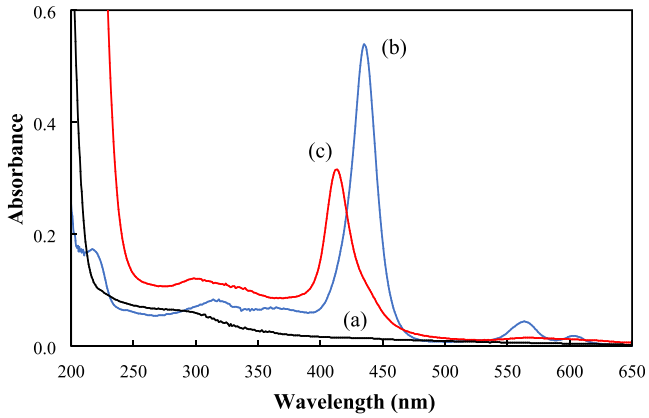

Figure 2. UV−vis absorption spectra of 0.5% (w/v) chitosan (a), 2 μmol/L VO(tpps) (b), and a chitosan-VO(tpps) conjugate (c) in an aqueous environment (pH 2.5).

Fourier transform infrared (FTIR) spectroscopy reveals the specific functional groups in chitosan and VO(tpps) that are involved in the formation of the chitosan-VO(tpps) complex. The electrostatic relationship between the NH_3^+ groups of chitosan and the SO_3^- groups of porphyrin is credited with the creation of chitosan-VO(tpps) complex.[38] The FTIR spectra of chitosan, VO(tpps), and the chitosan-VO(tpps) complex noted in KBr are given in Figure 3. Chitosan's absorption bands at 1153, 1091, 1031, and 894 cm^{-1} are typical backbone of the polysaccharide (Figure 3a). Chitosan's O−H (broad) and C−H(narrow) bands have respective stretching frequencies of 3417 and 2875 cm^{-1}. Two typical peaks were detected at 1649 and 1600 cm^{-1} for the stretching frequency of amide I (C═O) and amide II (N−H), respectively.[39] The O−H band of the $-SO_3H$ group in the VO(tpps) molecule was noted at 3450 cm^{-1} (Figure 3b) and transferred to 3421 cm^{-1} in the conjugate spectrum (Figure 3c). The electrostatic interaction between anionic VO(tpps) and cationic chitosan may explain this phenomenon. The band at 1024 cm^{-1} was ascribed to the

https://doi.org/10.1021/acsomega.3c05804
ACS Omega 2023, 8, 41612−41623

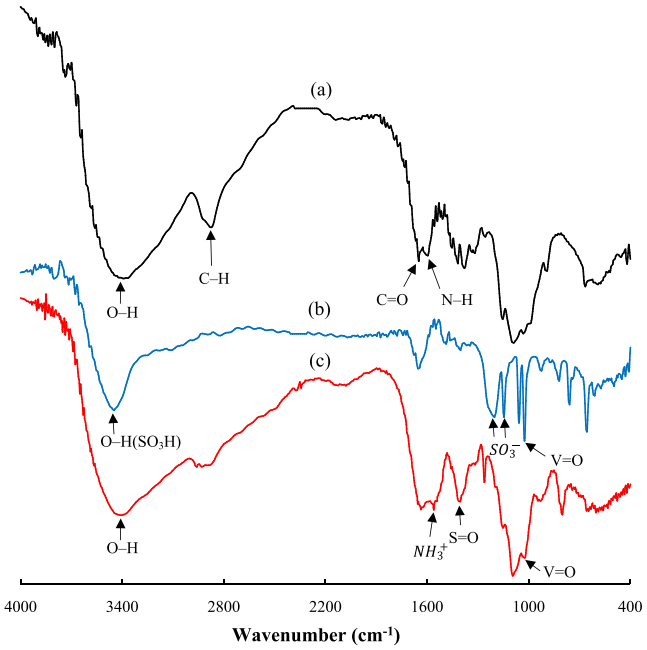

Figure 3. Chitosan (a), VOtpps (b), and chitosan-VOtpps complex (c) FTIR spectra noted in KBr.

stretching frequency of V═O in the VO(tpps) molecule[32]; this frequency was moved to 1033 cm^{-1} in the conjugate. The peaks of various phenyl groups at 900, 821, 740, and 632 cm^{-1} were displaced to smaller frequencies (5−12 cm^{-1}), indicating that the chitosan-VO(tpps) conjugate's macrocyclic core was disturbed.[38] The peaks at 1145 and 1205 cm^{-1} (Figure 3b) were ascribed to the symmetric and asymmetric stretching frequencies of the sulfonato group (SO_3^-) in VO(tpps).[40] In Figure 3c, the symmetric and asymmetric stretching bands of the sulfonato group (SO_3^-) were moved to 1033 and 1093 cm^{-1} with considerably attenuated N−H bands, suggesting that the SO_3^- groups of the VO(tpps) molecule participate actively in conjugation with chitosan.[34] Figure 3c depicts a wide peak at 1570 cm^{-1} that implies to the stretching frequency of NH_3^+ groups in the conjugate. The prominent peak at 1406 cm^{-1} (Figure 3c) ascribes to the stretching frequency of the S═O bond in the conjugate.[41] The ionic attraction between $NH_3^+$of chitosan and SO_3^- of VO(tpps) facilitates the formation of chitosan-VO(tpps) conjugate.[34,35,38] Figure 4 depicts the proposed structure of the chitosan-VO(tpps) conjugate.

Stability of Conjugate Chitosan-VO(tpps). To prevent VO(tpps) self-aggregation, an aqueous VO(tpps) solution (5 μmol/L) was steadily added to chitosan solution (1% w/v; pH 2.5) at a 1:1 (v/v) ratio with continuous magnetic stirring. Conjugation of VO(tpps) with chitosan occurred in an acidic aqueous environment due to the electrostatic attraction between the NH_3^+ and SO_3^- groups present in chitosan and VO(tpps). The stability of the complex was investigated in an acidic aqueous solution (pH 2.5) by measuring its kinetic UV−visible spectra at various time intervals. The UV−vis spectra of chitosan-VO(tpps) conjugate (Figure 5a) and the absorbance intensity of conjugate at 413 nm (Figure 5b) were found to be pretty steady in an acidic aqueous environment (pH 2.5), indicating that chitosan effectively increases the stability of VO(tpps) in acidic environments. By forming micelles, chitosan effectively protected Zn(tpps) in an acidic environ-

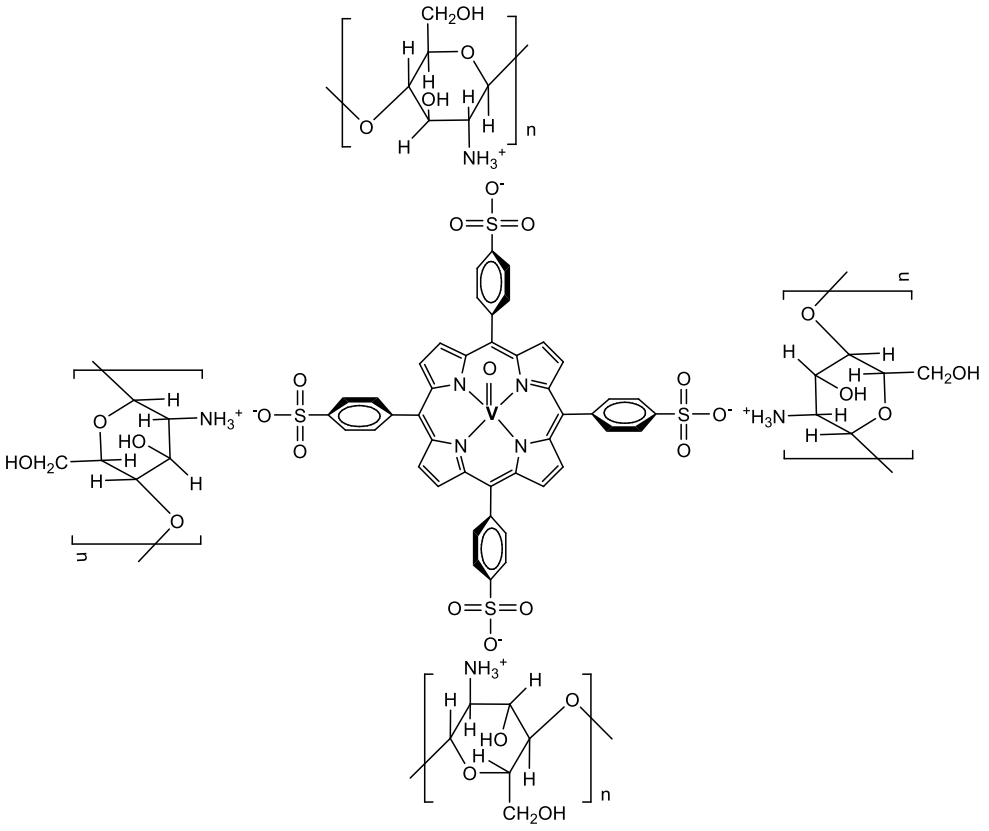

Figure 4. Proposed structure of the chitosan-VO(tpps) conjugate.

https://doi.org/10.1021/acsomega.3c05804
ACS Omega 2023, 8, 41612−41623

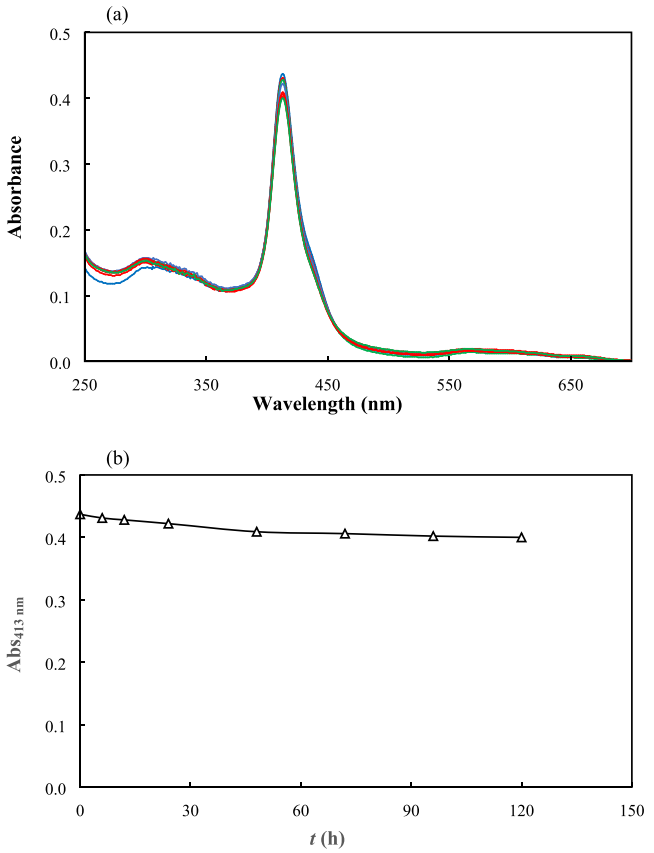

Figure 5. (a) Kinetic UV−vis absorption spectra of chitosan-VO(tpps) conjugate in an aqueous environment (pH 2.5) at various times. The conjugate absorption spectra were noted at 0, 6, 12, 24, 48, 72, 96, and 120 h. The VO(tpps) concentration in chitosan solution (0.5% (w/v); pH 2.5) was 2.5 μmol/L. (b) Kinetic trace at 413 nm of the chitosan-VO(tpps) conjugate. The data are extracted from Figure 5a.

ment from demetallization, as previously described.[34] It was also assumed that the cross-linked network of chitosan was responsible for Zn(tpps) segregation. The analogous mechanism may explain the stability of the chitosan-VO(tpps) conjugate in an acidic environment.

Impact of Contact Time. The influence of the interaction period on the kinetics and quantity of VO(tpps) conjugation with chitosan in an aqueous environment is illustrated in Figure 6. Initially, the conjugation rate between VO(tpps) and chitosan rises sharply but then decreases with time. It took 240−300 min for the conjugation rate between VO(tpps) and chitosan to attain equilibrium. Effective electrostatic magnetism among NH_3^+ and SO_3^- groups present in chitosan and VO(tpps), respectively, may account for the rapid conjugation at an early stage. As the chitosan surface became saturated, the rate of conjugation decreased, and VO(tpps) began penetrating chitosan pores at a very sluggish rate, as observed for Zn(tpps) and dye molecule conjugation with chitosan in aqueous solution.[34,42] Therefore, 300 min was chosen as the equilibrium time for maximal VO(tpps) conjugation.

Impact of the VO(tpps) Concentration. In order to study the dependence of VO(tpps) intensity on chitosan-VO(tpps) conjugation kinetics, the initial VO(tpps) concentration was varied from 2 to 10 μmol/L, whereas the other parameters remained constant. With increasing VO(tpps) intensity, the magnitude of VO(tpps) conjugated per unit

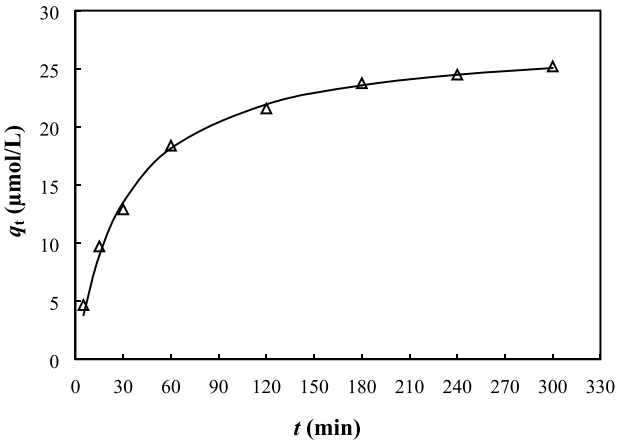

Figure 6. Influence of contact time on kinetics and quantity of VO(tpps) bound to chitosan in aqueous solution at the temperature of 30 °C (volume of solution: 40 mL, chitosan: 0.5% w/v, $[VO(tpps)]_0$: 4 μmol/L). The solid line was generated numerically using pseudo-second-order kinetics eq 2, and the values of k_2 and $q_{e(cal)}$ are stated in Table 1.

weight of chitosan boosted from 21.31 to 32.85 μmol/g, as depicted in Figure 7. This shows that the VO(tpps)

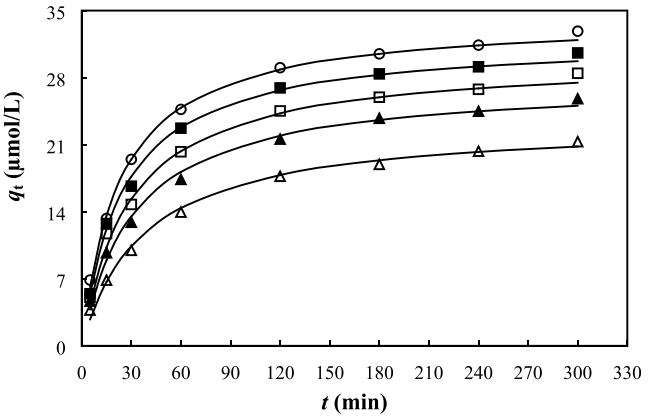

Figure 7. VO(tpps) conjugation with chitosan in aqueous solution at 30 °C (volume of solution: 40 mL; chitosan: 0.5% w/v; $[VO(tpps)]_0$: △: 2 μmol/L; ▲: 4 μmol/L; □: 6 μmol/L; ■: 8 μmol/L; and ○: 10 μmol/L. The solid line was calculated numerically using pseudo-second-order kinetic eq 2 and the values of k_2 and $q_{e(cal)}$ from Table 1.

concentration had an important impact on the conjugation process. The concentration gradient of VO(tpps) may be the source of a driving force that enhances VO(tpps) conjugation. Similar explanations have previously been provided for the conjugation of Zn(tpps),[34] reactive black 5 (RB5),[42] and H_2tpps[43] with chitosan in an aqueous medium.

Temperature Effect. Temperature effect analysis is required to design every bulk experiment. Experiments on the conjugation of VO(tpps) with chitosan were conducted at varying temperatures (30 to 45 °C). As shown in Figure 8, as the temperature of a solution increases, the equilibrium conjugation capacity increases slightly, representing an endothermic process. The negligible effect of temperature suggests that VO(tpps) conjugation with chitosan is a sluggish equilibrium process.[44] Similar behavior was noted in the conjugation of Zn(tpps) and anionic dye RB5 with chitosan in an aqueous environment.[34,42] The insignificant impact of

https://doi.org/10.1021/acsomega.3c05804
ACS Omega 2023, 8, 41612−41623

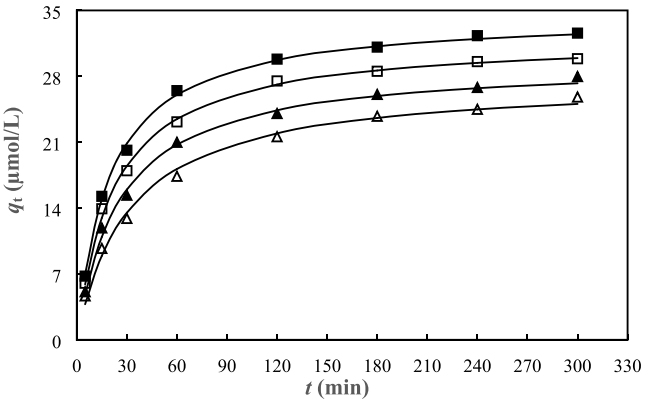

Figure 8. Influence of solution temperature on the kinetics and quantity of VO(tpps) bound to chitosan in an aqueous environment (volume of solution: 40 mL; chitosan: 0.05% w/v; $[VO(tpps)]_0$: 4 μmol/L; solution temperature: △, 30 °C; ▲, 35 °C; □, 40 °C; ■: 45 °C). The solid line was calculated numerically using pseudo-second-order kinetic eq 2 and the values of k_2 and $q_{e(cal)}$ from Table 1.

solution temperature on decolorization efficacy was also reported by other authors.[45]

Kinetic Analysis. To evaluate the kinetics involved in chitosan-VO(tpps) conjugation, well-known kinetic models, including pseudo-first-order,[46] pseudo-second-order,[47] and Elovich kinetic[48] models, were applied to examine data obtained from kinetic experiments. The equation of a pseudo-first-order model is given as follows:

$$\ln(q_e - q_t) = \ln q_e - k_1 t \quad (1)$$

where k_1 (min^{-1}) represents a pseudo-first-order conjugation rate constant estimated by plotting $\ln(q_e - q_t)$ against t.

The pseudo-second-order rate equation is expressed by eq 2:

$$q_t = \frac{k_2 q_e^2 t}{(1 + k_2 q_e t)} \quad (2)$$

where k_2 (g/μmol min) represents a pseudo-second-order conjugation rate constant computed from the linear expression imparted in the following eq 3:

$$\frac{t}{q_t} = \frac{1}{k_2 q_e^2} + \frac{1}{q_e} t \quad (3)$$

The eq 4 for the Elovich kinetic model is

$$q_t = \frac{1}{\beta}\ln(\alpha\beta) + \frac{1}{\beta}\ln t \quad (4)$$

where α (μmol/g min) represents the primary rate constant of VO(tpps) conjugation and β (g/μmol) is related to the extent of exterior expose and the activation energy for chemisorption. By plotting q_t versus ln$t$, we can determine the magnitudes of α and β can be determined.

The estimated kinetic results from the application of the kinetic equations are tabulated in Table 1. Typically, the optimal kinetic model is chosen on the basis of high correlation coefficients (R^2) and the similarity between theoretical and observed q_e values. The values of R^2 = 0.965 to 0.997 obtained from the pseudo-first-order model and the Elovich kinetic model (R^2 = 0.979 to 0.991) are trivial in comparison to the values of R^2 = 0.992 to 0.995 obtained from the pseudo-second-order model. The VO(tpps) conjugation data can be interpreted using a pseudo-second-order kinetic expression based on R^2 values and the similarity between theoretical and observed q_e values (Table 1). The good fit to the pseudo-second-order model suggests that the conjugation path is primarily driven by physisorption and is dependent on the electrostatic magnetism between the NH_3^+ and SO_3^- groups of chitosan and VO(tpps).[34,43,49] The high values of the Elovich rate constant (α) indicate the rapid conjugation of VO(tpps) at the beginning of the reaction (Figure 6), whereas the small values of the desorption constant (β) suggest the stability of the chitosan-VO(tpps) conjugate in the solution.[50−52]

Mechanism of Conjugation. To gain insight into the conjugation mechanism, experimental kinetic data were analyzed by two commonly employed diffusion models-film diffusion[53] and intraparticle diffusion.[54] The equations describing diffusion models are as follows:

Film diffusion model

$$\ln(1 - F) = -k_{fd} t \quad (5)$$

$$F = q_t/q_\infty \quad (6)$$

Intraparticle diffusion model

Table 1. Characteristics of the Kinetic Models Applied for the Assessment of Experimental Kinetic Data Acquired from Chitosan-VO(tpps) Conjugation at Various Concentrations of VO(tpps) and Solution Temperatures

parameters	[VO(tpps)] (μmol/L)					temperature (°C)			
	2.0	4.0	6.0	8.0	10.0	30	35	40	45
$q_{e\ (exp)}$ (μmol/g)	21.31	25.80	28.46	30.58	32.85	25.80	27.97	30.87	33.19
pseudo-first-order kinetic model									
$k_1 \times 10^{-3}$ (1/min)	10.20	10.20	10.00	10.20	10.40	10.20	10.40	10.20	10.80
$q_{e(cal)}$ (μmol/g)	15.89	18.28	19.62	19.44	20.30	18.28	18.04	18.67	18.89
R^2	0.977	0.991	0.997	0.995	0.995	0.991	0.985	0.990	0.965
pseudo-second-order kinetic model									
$k_2 \times 10^{-3}$ (g/μmol min)	1.13	1.14	1.15	1.26	1.27	1.24	1.32	1.40	1.46
$q_{e(cal)}$ (μmol/g)	23.42	27.70	30.12	32.15	34.36	27.70	29.59	32.15	34.60
R^2	0.993	0.993	0.992	0.994	0.994	0.993	0.995	0.994	0.995
Elovich kinetic model									
α (μmol/g min)	1.80	2.82	3.77	5.77	7.28	2.82	4.25	7.29	12.07
β (g/μmol)	0.23	0.21	0.20	0.20	0.19	0.21	0.20	0.20	0.20
R^2	0.979	0.985	0.986	0.984	0.985	0.985	0.991	0.989	0.984

https://doi.org/10.1021/acsomega.3c05804
ACS Omega 2023, 8, 41612−41623

$$q_t = k_{id} t^{0.5} + I \quad (7)$$

where k_{fd} (1/min) and k_{id} (μmol/g min$^{0.5}$) are film diffusion and intraparticle diffusion rate constants, respectively. F is a fractional quantity conjugated at equilibrium that can be calculated using the ratio q_t/q_∞, where q_t (μmol/g) and q_∞ (μmol/g) are the extent of VO(tpps) conjugated with chitosan at t time and infinite time, respectively. In eq 7, the intercept is represented by I (μmol/g), which gives evidence regarding the width of the frontier layer. Figure 9 depicts typical plots of

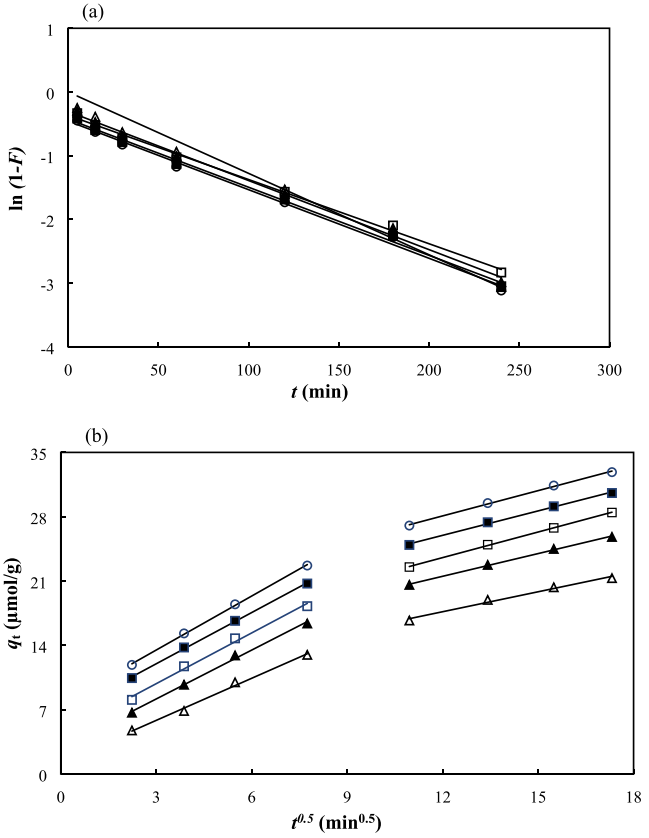

Figure 9. Characteristic charts of $\ln(1 - F)$ versus t (a) and q_t versus $t^{0.5}$ (b) for chitosan-VO(tpps) conjugation in the aqueous environment at five different concentrations of VO(tpps) (solution volume: 40 mL; chitosan: 0.5% w/v; $[VO(tpps)]_0$: △: 2 μmol/L; ▲: 4 μmol/L; □: 6 μmol/L; ■: 8 μmol/L; ○: 10 μmol/L).

applied diffusion models. Figure 9a displays specific plots of the film diffusion model, $\ln(1 - F)$ versus t, for the chitosan-VO(tpps) conjugates in aqueous environments at varying VO(tpps) concentrations. The absence of any line passing through the origin is indicative that film diffusion alone does not solely control the chitosan-VO(tpps) conjugation process. The values of k_{fd} and correlation coefficient (R^2) acquired from the film diffusion model are presented in Table 2. In Figure 9b, all the plots of the intraparticle diffusion model, namely q_t versus $t^{0.5}$, exhibit two linear regions with distinct slopes. This implies that there are two phases in the conjugation process. The first linear region was attributed primarily to external surface conjugation or macro pore diffusion with a rate constant k_{id1} (μmol/g min$^{0.5}$), whereas the second linear region was attributed to a progressive diffusion into the interior surface of chitosan with a rate constant k_{id2}. Similar explanations for this phenomenon were previously reported.[34,55,56]

Conjugation Isotherm. To predict the nature of the interaction between VO(tpps) and chitosan, bulk equilibrium data were tested with the most prevalent isotherm models. Figure 10 illustrates the correlation between q_e and C_e. The

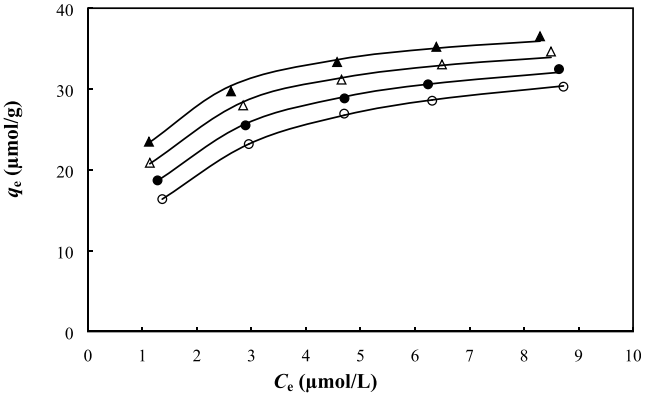

Figure 10. Conjugation isotherms of chitosan-VO(tpps) conjugate in aqueous medium at various temperatures (volume of solution: 40 mL; $[VO(tpps)]_0$: 2−10 μmol/L; chitosan concentration: 0.5% w/v; solution temperature: ○: 30 °C; ●: 35 °C; △: 40 °C; ▲: 45 °C). The Langmuir isotherm eq 12 is used to generate all solid lines numerically.

graph demonstrated that a rise in solution temperature increases the extent of VO(tpps) conjugation, indicating that the conjugation process is endothermic.

The Freundlich,[57] Temkin,[58] and Langmuir[59] isotherm equations were used to study the bulk conjugation experiment data and determine the most appropriate model. Following are the equations of the employed isotherm models:

Freundlich model:

Table 2. Estimated Values of Diffusion Parameter for VO(tpps) Conjugation with Chitosan in Aqueous Solution at Various Concentrations of VO(tpps) and Solution Temperatures

parameters	[VO(tpps)] concentration (μmol/L)					temperature (°C)			
	2.0	4.0	6.0	8.0	10.0	30	35	40	45
film diffusion model									
$k_{fd} \times 10^{-2}$ (1/min)	1.15	1.08	1.01	1.07	1.08	2.58	1.75	1.95	1.83
R^2	0.996	0.995	0.995	0.996	0.995	0.985	0.993	0.994	0.984
intraparticle diffusion model									
k_{id1} (μmol/g min$^{0.5}$)	1.53	1.77	1.84	1.86	1.96	1.77	1.93	1.83	1.75
R^2	0.994	0.997	0.992	0.999	0.999	0.997	0.994	0.984	0.992
k_{id2} (μmol/g min$^{0.5}$)	0.72	0.82	0.93	0.89	0.92	0.82	0.78	0.86	0.87
R^2	0.986	0.998	0.999	0.997	0.998	0.998	0.997	0.997	0.984

https://doi.org/10.1021/acsomega.3c05804
ACS Omega 2023, 8, 41612−41623

Table 3. Isotherm Constants for the Conjugation of VOtpps with Chitosan at Varied Temperatures

isotherm models	parameters	temperatures (°C)			
		30	35	40	45
Freundlich	K_F ($(\mu mol/g)(\mu mol/L)^{-1/n}$)	15.39	17.98	20.72	23.36
	n	2.99	3.45	3.96	4.51
	R^2	0.967	0.977	0.982	0.985
Temkin	K_T (μmol/L)	6.77	10.98	19.48	33.50
	b_T (J/mol)	331.73	354.17	380.07	403.04
	R^2	0.989	0.994	0.995	0.996
Langmuir	K_L (L/g)	0.61	0.81	1.09	1.31
	$a_L \times 10^{-2}$ (L/μmol)	1.69	2.22	2.89	3.35
	q_m (μmol/g)	36.10	36.63	37.59	39.22
	R^2	1.0	0.999	0.997	0.994
thermodynamics	ΔG (kJ/mol)	−24.52	−25.63	−26.73	−27.75
	ΔH (kJ/mol)	37.30			
	ΔS (J/mol K)	204.22			
	R^2	0.987			

Nonlinear form

$$q_e = K_F C_e^{1/n} \tag{8}$$

Linear form

$$\ln q_e = \frac{1}{n}\ln C_e + \ln K_F \tag{9}$$

Temkin model:
Nonlinear form

$$q_e = \frac{RT}{b_T}\ln(K_T C_e) \tag{10}$$

Linear form

$$q_e = \frac{RT}{b_T}\ln K_T + \frac{RT}{b_T}\ln C_e \tag{11}$$

Langmuir model:
Nonlinear form

$$q_e = \frac{K_L C_e}{(1 + a_L C_e)} \tag{12}$$

Linear form

$$\frac{C_e}{q_e} = \frac{1}{K_L} + \frac{a_L}{K_L} C_e \tag{13}$$

where C_e (μmol/L) represents the equilibrium concentration of VO(tpps) and q_e (μmol/g) represents the VO(tpps) conjugation ability of chitosan at equilibrium. The Freundlich constants K_F ($(\mu mol/g)(\mu mol/L)^{-1/n}$) and n represent the capacity and potency of VO(tpps) conjugation. The constant of the Temkin equation is K_T (μmol/L), b_T (J/mol) is a measure of the heat of conjugation, R (8.314 J/mol K) is the universal gas constant, and T (K) is the absolute temperature. The ratio of Langmuir isotherm constants (K_L/a_L) characterizes the upper limit of chitosan's conjugation capacity, q_m (μmol/g). In Table 3, the parameters of the isotherms are enumerated. The Langmuir isotherm equation adequately explains the equilibrium behavior of chitosan-VO(tpps) conjugation based on the magnitudes of R^2. The Freundlich isotherm parameter n was calculated to be greater than one, indicating that conjugation between chitosan and VO(tpps) is favorable.[34,43] At 30 to 45 °C, the maximal amount of VO(tpps) conjugated with chitosan was estimated to be between 36.10 and 39.22 μmol/g. However, at 30 and 45 °C, the maximal amount of Zn(tpps) bound to chitosan was determined to be 135.14 and 151.52 mol/g, respectively.[34]

Separation factor (R_L) is a dimensionless constant, which represents the fundamental features of the Langmuir equation, which is stated as follows:

$$R_L = \frac{1}{(1 + a_L C_0)} \tag{14}$$

where a_L (L/μmol) represents the Langmuir isotherm constant and C_0 (μmol/L) represents the maximum initial concentration of VO(tpps) used in conjugation experiments. Separation factor (R_L) values imply the nature of conjugation ($R_L > 1.0$ indicates an unfavorable interaction; $0 < R_L < 1.0$ implies a promising interaction). The values of R_L for chitosan-VO(tpps) conjugate at 30, 35, 40, and 45 °C were estimated to be 0.855, 0.818, 0.776, and 0.749, respectively, indicating favorable conjugation at all of the aforementioned temperatures.[60] Three error functions, including the sum of squares of errors (SSE), the sum of absolute errors (SAE), and the average relative errors (ARE), were considered to determine the isotherm model that best fits the present conjugation process.[61] Freundlich, Temkin, and Langmuir isotherms were subjected to error analysis (Table 4). In addition, error analysis data revealed that the Langmuir isotherm model provided the best fit for chitosan-VO(tpps) conjugation in an aqueous medium.

Parameters for Activation and Thermodynamics. The activation energy (E_a) for the studied conjugation system was determined using the values of k_2 imparted in Table 1 at various temperatures of the solution. The correlation between activation energy (E_a), rate constant (k_2), and solution temperature (T) according to the Arrhenius equation is as follows:

$$\ln k_2 = -\frac{E_a}{R}\left(\frac{1}{T}\right) + \text{Constant} \tag{15}$$

where R (8.314 J/mol K) represents the constant for an ideal gas. The activation energy (E_a) at 30−45 °C was determined using the Arrhenius plot of $\ln k_2$ versus $1/T$ ($R^2 = 0.997$) when the VO(tpps) concentration was 4 μmol/L in an aqueous medium. The computed E_a value of 8.78 kJ/mol suggests that

https://doi.org/10.1021/acsomega.3c05804
ACS Omega 2023, 8, 41612−41623

Table 4. Isotherm Error Analysis for Chitosan-VO(tpps) Conjugation in Aqueous Solution

isotherm models	temperatures (°C)	errors		
		SSE	SAE	ARE
Freundlich	30	5.131	4.408	3.613
Temkin		1.381	2.350	1.981
Langmuir		0.059	0.398	0.285
Freundlich	35	3.199	3.469	2.639
Temkin		0.721	1.693	1.334
Langmuir		0.235	0.839	0.583
Freundlich	40	2.502	3.222	2.242
Temkin		0.554	1.551	1.110
Langmuir		0.485	1.407	1.047
Freundlich	45	1.882	2.729	1.768
Temkin		0.468	1.376	1.205
Langmuir		0.371	1.284	1.176

VO(tpps) conjugation with chitosan is a physisorption mechanism.[34]

Using the following equations,[43] the thermodynamic activation parameters of VO(tpps) conjugation with chitosan, including enthalpy ($\Delta H^{\ddagger}$), entropy ($\Delta S^{\ddagger}$), and Gibb's free energy ($\Delta G^{\ddagger}$), were estimated:

$$\ln\left(\frac{k_2}{T}\right) = -\frac{\Delta H^{\ddagger}}{R}\left(\frac{1}{T}\right) + \ln\left(\frac{k_B}{h_P}\right) + \frac{\Delta S^{\ddagger}}{R} \quad (16)$$

$$\Delta G^{\ddagger} = \Delta H^{\ddagger} - T\Delta S^{\ddagger} \quad (17)$$

where k_2, R, and T have the same meaning as previously mentioned, k_B represents the Boltzmann constant (1.381×10^{-23} J/K), and h_P represents the Planck constant (6.626×10^{-34} J s). From the slope and intercept of the linear plot of $\ln(k_2/T)$ versus $1/T$ ($R^2 = 0.994$), $\Delta H^{\ddagger}$ (6.20 kJ/mol) and $\Delta S^{\ddagger}$ (−280.21 J/mol K) values of the conjugation process were calculated.

The estimated $\Delta H^{\ddagger}$ value of conjugation (≤40 kJ/mol) indicates physical binding of VO(tpps) with chitosan, which was confirmed by the E_a value (8.78 kJ/mol).[62] The positive value of $\Delta H^{\ddagger}$ (6.20 kJ/mol) also implies that the conjugation process is endothermic.[63] Based on the $\Delta S^{\ddagger}$ value (−280.21 J/mol K), it can be concluded that the VO(tpps) conjugation did not significantly alter the internal structure of chitosan.[64] Negative $\Delta S^{\ddagger}$ also indicates that VO(tpps) conjugation occurs via an associative mechanism in which individual VO(tpps) molecules remain intact.[65] The estimated value of $\Delta S^{\ddagger}T_{av}$ was found to be greater than $\Delta H^{\ddagger}$, indicating an entropy-driven activation process,[34,66] where T_{av} represents the mean of the studied temperatures. Positive $\Delta G^{\ddagger}$ values (91.10, 92.50, 93.90, and 95.30 kJ/mol) at the investigated temperatures (30, 35, 40, and 45 °C) indicate that the chitosan-VO(tpps) conjugation system contains an energy barrier. This phenomenon is quite typical and logical as the actuated compound is an agitated form in the transition state.

Using the following expressions,[67] the thermodynamic parameters of VO(tpps) conjugation with chitosan, including variations in Gibb's free energy (ΔG), entropy (ΔS), and enthalpy (ΔH), were estimated.

$$\Delta G = -RT\ln a_L \quad (18)$$

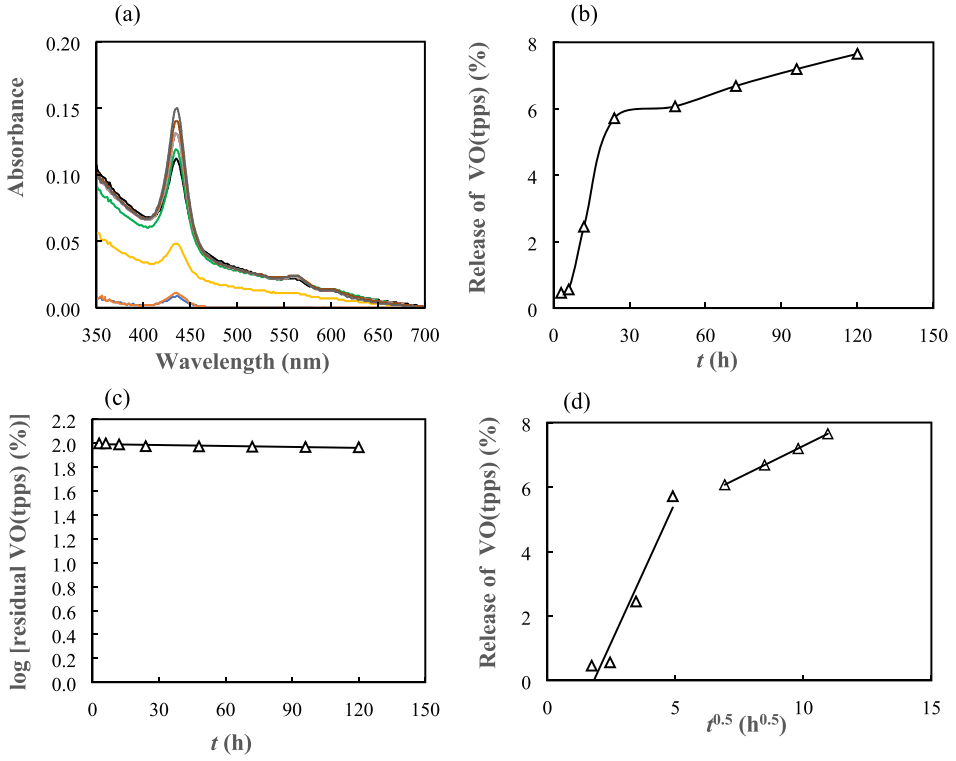

Figure 11. (a) Usual UV−vis spectra of VO(tpps) liberated from chitosan-VO(tpps) conjugate at different intervals of time in 0.1 mol/L phosphate buffer (pH 7.4) at 37 °C; (b) in vitro discharge profile of VO(tpps) from chitosan-VO(tpps) conjugate in 0.1 mol/L phosphate buffer (pH 7.4) at 37 °C; (c) plot of log [residual VO(tpps) (%)] vs time (data are taken from Figure 11b); and (d) plot of VO(tpps) release (%) vs square root of time (data are taken from Figure 11b).

https://doi.org/10.1021/acsomega.3c05804
ACS Omega 2023, 8, 41612−41623

$$\ln a_L = \frac{\Delta S}{R} - \frac{\Delta H}{RT} \quad (19)$$

where a_L, T, and R have the same meaning as previously mentioned. By plotting $\ln a_L$ versus $1/T$ (R^2 = 0.987; figure not given), the slope and intercept were employed to estimate the extent of enthalpy (ΔH) and entropy (ΔS), respectively. Table 3 provides a summary of the thermodynamic parameter values obtained. The magnitude of ΔH (37.3 kJ/mol) indicates that the chitosan-VO(tpps) conjugation is endothermic, which is confirmed by the increase in the equilibrium conjugation of VO(tpps) with temperature. The negative calculated ΔG values (−24.52 to −27.55 kJ/mol) at the investigated temperatures (30 to 45 °C) indicate that the conjugation between VO(tpps) and chitosan is spontaneous. VO(tpps) conjugation with chitosan is anticipated to be favorable at elevated temperatures[34,43] based on the positive ΔS value (204.22 J/mol K), which is also supported by the positive ΔH values.

Release of VO(tpps) In Vitro from the Chitosan-VO(tpps) Conjugate. The dialysis procedure was used to investigate the liberation of VO(tpps) from the chitosan-VO(tpps) conjugate in 0.1 mol/L phosphate buffer (pH 7.4). In a dialysis tube (MWCO ≤ 14,000 Da), 50 mg of the conjugate and 3 mL of the buffer were incubated in a vial containing 37 mL of the same buffer solution. A magnetic stir bar was utilized to agitate the system at 150 rpm at 37 °C. Using spectrophotometry, the concentration of VO(tpps) released from the conjugate in the buffer solution was determined. Figure 11a depicts the typical UV−visible spectra of VO(tpps) liberated from the chitosan-VO(tpps) conjugate in 0.1 mol/L phosphate buffer (pH 7.4). The concentration of VO(tpps) was found to increase progressively in the outer buffer solution. However, only 7.65% of VO(tpps) was released within 120 h from the conjugate (Figure 11b). The strong electrostatic attraction between the NH_3^+ and SO_3^- groups of chitosan and VO(tpps) was primarily responsible for the slow discharge of VO(tpps) from the chitosan-VO(tpps) conjugate.[34,68] The plot of logarithmic residual VO(tpps) percentage in conjugate versus time in Figure 11c indicates that the kinetics of VO(tpps) liberation did not obey the first-order equation (R^2 = 0.761). Figure 11d demonstrates that VO(tpps) was liberated from the conjugate in two distinct phases. The first linear region (R^2 = 0.947) was primarily attributed to the release of adsorbed or entrapped VO(tpps) from the chitosan surface, whereas the second linear region (R^2 = 1.000) was attributed to the diffusion of VO(tpps) from the distended chitosan matrix.[69] The kinetics of VO(tpps) release appears to conform more closely to the Higuchi model than to the first-order kinetics, indicating that the chitosan-VO(tpps) conjugate is a matrix type rather than a reservoir type.

CONCLUSIONS

UV−visible and FTIR spectrophotometric techniques were utilized to validate the conjugation of chitosan with insulin-mimetic VO(tpps). Chitosan-VO(tpps) conjugate was formed in the aqueous environment due to electrostatic attraction between NH_3^+ and SO_3^- groups of chitosan and VO(tpps), respectively. Chitosan increases the stability of VO(tpps) in extremely acidic environments. The conjugation between chitosan and VO(tpps) was anticipated to influence the solution's concentration and temperature. The VO(tpps) assimilation capacity of chitosan intensified with increasing temperature (30 to 45 °C) and VO(tpps) solution concentration (2 to 10 μmol/L). The pseudo-second-order kinetic equation correlates better with kinetic data than the pseudo-first-order and Elovich models. The Langmuir isotherm accurately described the isotherm data of VO(tpps) conjugation (R^2 = 0.994 to 1.0). According to the Langmuir equation, the maximal conjugation capacity of VO(tpps) was calculated to be 39.22 μmol/g at 45 °C. The conjugation system is spontaneous and endothermic according to thermodynamic analyses. The liberation of VO(tpps) from the chitosan-VO(tpps) conjugate was evaluated in 0.1 mol/L phosphate buffer solution (pH 7.4) at 37 °C. Kinetic analysis of experimental release data revealed that the release of VO(tpps) from the conjugate was a two-stage process, which is best described by the Higuchi model. Chitosan could potentially be used as an effective carrier agent for the development of a solution and solid insulin-mimetic chitosan-VO(tpps) conjugate, as indicated by the experimental results.

EXPERIMENTAL SECTION

Materials. The chitosan was provided by Katokichi Bio Co. Ltd. and used exactly as received. Frontier Scientific Inc. of Utah, United States, supplied *meso*-tetrakis(4-sulfonatophenyl)porphyrin, H_2(tpps). The vanadium(IV) oxide sulfate was acquired from Japan's Wako purified chemical industries. The Sephadex LH-20 supplied by Amersham Pharmacia Biotech was utilized as the stationary phase of column chromatography for the separation of VO(tpps) from the reaction mixture. Dialysis membranes were obtained from Medicell International Ltd., London. This study employed deionized water. This experiment utilized only substances of analytical grade.

Synthesis of Complex VO(tpps). The synthesis of VO(tpps) from H_2(tpps) was conducted with minor modifications as previously reported.[32] H_2tpps (1.1131 g) and $VOSO_4.5H_2O$ (2.8839 g) were refluxed with agitation for 24 h at 150 °C in 250 mL of *N*,*N*-dimethylformamide. The solution was subjected to evaporation until it reached a volume of approximately 5 mL and passed through the Sephadex LH-20-packed glass column. To prevent photodegradation, the isolated VO(tpps) solution was evaporated to dryness and stored in a dark amber glass vial. Elemental analysis of $C_{44}H_{28}O_{12}S_4N_4VO{\cdot}8H_2O{\cdot}2C_3H_7NO$, VO(tpps), calculated (%): C 46.55, H 4.53, N 6.51; observed (%): C 46.21, H 4.48, N 6.55.[32]

Preparation of Chitosan-VO(tpps) Conjugate. The synthesis of chitosan-VO(tpps) conjugate was conducted in an aqueous medium with minor modifications as previously reported.[34] A 1% chitosan solution was made by mixing 5 g of chitosan with 500 mL of diluted acetic acid (pH 2.5) and stirring the mixture for 2 h at 30 °C. While continuously agitating, the freshly prepared chitosan solution and a 500 μmol/L aqueous solution of VO(tpps) were mixed in a 1:1 (v/v) ratio. This was done slowly to prevent the self-aggregation of VO(tpps). To enable the conjugation between chitosan and the VO(tpps) molecule, the solution was preserved at 30 °C for 8 h with constant magnetic stirring. By means of dialysis, the unconjugated VO(tpps) were removed from the melange. The resulting chitosan-VO(tpps) conjugate solution was desiccated in an electric furnace at 70 °C and kept in an orange glass container.

Spectroscopic Investigations. The UV−vis spectra of chitosan, VO(tpps), and the chitosan-VO(tpps) complex were

https://doi.org/10.1021/acsomega.3c05804
ACS Omega 2023, 8, 41612−41623

measured in an aqueous environment using a UV-1900i spectrophotometer (Shimadzu, Japan) at a wavelength range of 200−800 nm and a quartz cuvette with a width of 1 cm. Prior to each sample run, the zero line of the UV−vis spectrophotometer was corrected with the respective medium.

The FTIR spectra of chitosan, VO(tpps), and the chitosan-VO(tpps) complex were measured by using an IRPrestige-21 FTIR spectrophotometer (Shimadzu, Japan) with a range of 400−4000 cm^{-1}. The solid materials were finely milled and mixed with potassium bromide (KBr) in a 1:100 ratio to create a translucent disk.

Preparing the Membrane. Dialysis tube (10 × 2.5 cm) of Visking dialysis flat membranes (Medicell International Ltd., London, SE8 3FD; MWCO ≤ 14,000 Da) was dipped in deionized water for 8 h while being agitated at 35 °C. Every hour, the media water was altered with fresh deionized water to eradicate any water-soluble foreign materials. The dialysis conduit was then immersed in 60 °C water for 2 min. The membrane tube was then immersed for 30 min in 70% aqueous methanol. The dialysis tube was stored in a 50% methanol aqueous solution until the experiment.

Studies of Batch Equilibrium. At room temperature, 37 mL of aqueous VO(tpps) solution was placed in a 125 mL stoppered vial to conduct a batch conjugation experiment. Chitosan aqueous solution (0.5% w/v; 3 mL) was taken in a membrane tube and dipped in 37 mL of a VO(tpps) solution (4 μmol/L). Each bottle's closure was secured to prevent solvent evaporation. The sample containers were stirred (150 r/min) in a thermostatic water bath at 30 °C until attained the equilibrium. Sample containers were removed from the water immersion at predetermined intervals, and the quantity of VO(tpps) conjugated with chitosan was determined spectrophotometrically using a UV-1900i Shimadzu spectrophotometer with a λ_{max} value of 436 nm.[34] At 436 nm, the molar absorption coefficient of VO(tpps) in aqueous solution was determined to be 1.84 × 10^5 L/mol.cm. The extent of VO(tpps) conjugated with chitosan at any time t, q_t (μmol/g) was calculated by using eq 20:

$$q_t = \frac{V(C_0 - C_t)}{m} \tag{20}$$

where C_0 (μmol/L) is the VO(tpps) concentration in solution at time zero, C_t (μmol/L) represents the VO(tpps) concentration in outer membrane solution at time t, V (L) represents the solution volume, and m (g) represents the weight of chitosan.

The kinetic experiment was conducted at changing concentrations of VO(tpps) (2−10 μmol/L) and temperatures of the solution (30−45 °C). Additionally, the conjugation equilibrium experiment was conducted at varying solution temperatures (30−45 °C).

The quantity of VO(tpps) conjugated with chitosan at equilibrium, q_e (μmol/g), was calculated by

$$q_e = \frac{V(C_0 - C_e)}{m} \tag{21}$$

where C_e (mol/L) is the VO(tpps) concentration in the outer membrane solution at equilibrium; as indicated previously, C_0, V, and m are the same.

Studies of VO(tpps) Release In Vitro. The VO(tpps) release experiment was performed in 0.1 mol/L phosphate buffer (pH 7.4 at 37 °C) using a dialysis procedure with a bag of dialysis membrane (MWCO ≤ 14,000 Da).[34] One end of the dialysis tube was secured with thread, and 50 mg of solid chitosan-VO(tpps) complex and 3 mL of buffer solution were placed inside. The other end of the tube was then knotted and plunged into the same buffer solution (37 mL) in a bottle with a stopper. At 37 °C, the corked bottle was magnetically agitated at 150 r/min. At various time intervals, the concentration of VO(tpps) in the outer solution of the dialysis membrane was determined using a spectrophotometer. After each measurement, the removed solution was reintroduced into the system. All experimental data provided in this article represent the mean of two separate analyses.

AUTHOR INFORMATION

Corresponding Authors

Subarna Karmaker − *Department of Chemistry, Jahangirnagar University, Dhaka 1342, Bangladesh*; Email: ksubarna_ju@yahoo.com

Tapan Kumar Saha − *Department of Chemistry, Jahangirnagar University, Dhaka 1342, Bangladesh*; orcid.org/0000-0002-1333-8014; Phone: (+880) 2 224491045-51 (PABX) Extn. 1437; Email: tksaha_ju@yahoo.com; Fax: (+880) 2 224491052

Authors

Chironjit Kumar Shaha − *Department of Chemistry, Jahangirnagar University, Dhaka 1342, Bangladesh; Veterinary Drug Residue Analysis Division, Institute of Food and Radiation Biology, Atomic Energy Research Establishment (AERE), Dhaka 1349, Bangladesh*

Bithy Sarker − *Department of Chemistry, Jahangirnagar University, Dhaka 1342, Bangladesh*

Shurid Kishore Mahalanobish − *Department of Chemistry, Jahangirnagar University, Dhaka 1342, Bangladesh*

Md. Sharif Hossain − *Department of Biotechnology & Genetic Engineering, Jahangirnagar University, Dhaka 1342, Bangladesh*

Complete contact information is available at: https://pubs.acs.org/10.1021/acsomega.3c05804

Notes

The authors declare no competing financial interest.

ACKNOWLEDGMENTS

We are grateful for the support provided by Jahangirnagar University (T.K.S.), the Ministry of Science and Technology, Government of the People's Republic of Bangladesh (S.K.), and the Alexander von Humboldt Foundation (ref.34-8151/T.K.S. (GA-Nr. 20 007)) in Germany.

REFERENCES

(1) Wang, Y.; Wu, C. Site-specific conjugation of polymers to proteins. *Biomacromolecules* **2018**, *19*, 1804−1825.

(2) Confederat, L. G.; Motrescu, I.; Condurache, M. I.; Constantin, S.; Bujor, A.; Tuchilus, C. G.; Profire, L. Chitosan-based delivery systems loaded with glibenclamide and lipoic acid: Formulation, characterization, and kinetic release studies. *Appl. Sci.* **2020**, *10*, 7532.

(3) Constantin, S. M.; Buron, F.; Routier, S.; Vasincu, I. M.; Apotrosoaei, M.; Lupascu, F.; Confederat, L.; Tuchilus, C.; Constantin, M. T.; Sava, A.; Profire, L. Formulation and characterization of new polymeric systems based on chitosan and xanthine derivatives with thiazolidin-4-one scaffold. *Materials* **2019**, *12*, 558.

(4) Ekladious, I.; Colson, Y. L.; Grinstaff, M. W. Polymer−drug conjugate therapeutics: advances, insights and prospects. *Nat. Rev. Drug Discovery* **2019**, *18*, 273−294.
(5) Chytil, P.; Koziolová, E.; Etrych, T.; Ulbrich, K. HPMA copolymer-drug conjugates with controlled tumor-specific drug release. *Macromol. Biosci.* **2018**, *18*, No. 1700209.
(6) Minrath, I.; Arbeiter, D.; Schmitz, K.; Sternberg, K.; Petersen, S. *In vitro* characterization of polyacrylamide hydrogels for application as implant coating for stimulus-responsive local drug delivery. *Polym. Adv. Technol.* **2014**, *25*, 1234−1241.
(7) Kumar, T. M. P.; Umesh, H. M.; Shivakumar, H. G.; Ravi, V.; Siddaramaiah. Feasibility of Polyvinyl Alcohol as a Transdermal Drug Delivery System for Terbutaline Sulphate. *J. Macromol. Sci., Part A: Pure Appl. Chem.* **2007**, *44*, 583−589.
(8) Karmaker, S.; Saha, T. K.; Yoshikawa, Y.; Yasui, H.; Sakurai, H. A novel drug delivery system for type 1 diabetes: Insulin-mimetic vanadyl-poly(γ-glutamic acid) complex. *J. Inorg. Biochem.* **2006**, *100*, 1535−1546.
(9) Saha, T. K.; Ichikawa, H.; Fukumori, Y. Gadolinium diethylenetriaminopetaaceitic acid-loaded chitosan microspheres for gadolinium neutron-capture therapy. *Carbohydr. Res.* **2006**, *341*, 2835−2841.
(10) Elieh-ali-komi, D.; Hamblin, M. R. Chitin and chitosan: Production and application of versatile biomedical nanomaterials. *Int. J. Adv. Res.* **2016**, *4*, 411−427.
(11) Bernkop-schnürch, A.; Dünnhaupt, S. Chitosan-based drug delivery systems. *Eur. J. Pharm. Biopharm.* **2012**, *81*, 463−469.
(12) (a) Elwakeel, K. Z.; Abd el-ghaffar, M. A.; El-kousy, S. M.; El-shorbagy, H. G. Synthesis of new ammonium chitosan derivatives and their application for dye removal from aqueous media. *Chem. Eng. J.* **2012**, *203*, 458−468. (b) Saigl, Z.; Tifouti, O.; Alkhanbashi, B.; Alharbi, G.; Algamdi, H. Chitosan as adsorbent for removal of some organic dyes: a review. *Chem. Pap.* **2023**, *77*, 2363−2405.
(13) (a) Elwakeel, K. Z. Removal of Cr(VI) from alkaline aqueous solutions using chemically modified magnetic chitosan resins. *Desalination* **2010**, *250*, 105−112. (b) Wang, K.; Zhang, F.; Xu, K.; Che, Y.; Qi, M.; Song, C. Modified magnetic chitosan materials for heavy metal adsorption: a review. *RSC Adv.* **2023**, *13*, 6713−6736.
(14) Karimi-maleh, H.; Ayati, A.; Davoodi, R.; Tanhaei, B.; Karmi, F.; Malekmohammadi, S.; Orooji, Y.; Fu, L.; Sillanpaa, M. Recent advances in using chitosan-based adsorbents for removal of pharmaceutical contaminants: A review. *J. Clean. Prod.* **2021**, *291*, No. 125880.
(15) Sarkar, S.; Das, D.; Dutta, P.; Kalita, J.; Wann, S. B.; Manna, P. Chitosan: A promising therapeutic agent and effective drug delivery system in managing diabetes mellitus. *Carbohydr. Polym.* **2020**, *247*, No. 116594.
(16) Seo, M. H.; Park, J. H.; Kwak, H. S. Antidiabetic activity of nanopowdered chitosan in db/db mice. *Food Sci. Biotechnol.* **2010**, *19*, 1245−1250.
(17) Hayashi, K.; Ito, M. Antidiabetic action of low molecular weight chitosan in genetically obese diabetic KK-Ay mice. *Biol. Pharm. Bull.* **2002**, *25*, 188−192.
(18) Yu, X.; Wen, T.; Cao, P.; Shan, L.; Li, L. Alginate-chitosan coated layered double hydroxide nanocomposites for enhanced oral vaccine delivery. *J. Colloid Interface Sci.* **2019**, *556*, 258−265.
(19) Confederat, L. G.; Motrescu, I.; Condurache, M. I.; Constantin, S.; Bujor, A.; Tuchilus, C. G.; Profire, L. Chitosan-Based Delivery Systems Loaded with Glibenclamide and Lipoic Acid: Formulation, Characterization, and Kinetic Release Studies. *Appl. Sci.* **2020**, *10*, 7532.
(20) Lupascu, F.; Confederat, L.; Sandra, C.; Stan, C. I.; Sava, A.; Avram, I.; Lupusoru, E. C.; Profire, L. Biological evaluation of chitosan-antidiabetic drug formulations for the treatment of diabetes mellitus. *Farmacia* **2017**, *65*, 508−514.
(21) Constantin, S. M.; Lupascu, F. G.; Apotrosoaei, M.; Focsa, A. V.; Vasincu, I. M.; Confederat, L. G.; Dimitriu, G.; Lupusoru, C. E.; Routier, S.; Buron, F.; Profire, L. Antidiabetic effects and safety profile of chitosan delivery systems loaded with new xanthine-thiazolidine-4-onederivatives: *In vivo* studies. *J. Drug Delivery Sci. Technol.* **2020**, *60*, No. 102091.
(22) Saha, T. K.; Frauendorf, H.; John, M.; Dechert, S.; Meyer, F. Efficient oxidative degradation of azo dyes by a water-soluble manganese porphyrin catalyst. *Chem. Catal. Chem.* **2013**, *5*, 796−805.
(23) Varchi, G.; Foglietta, F.; Canaparo, R.; Ballestri, M.; Arena, F.; Sotgiu, G.; Fanti, S. Engineered porphyrin loaded core-shell nanoparticles for selective sonodynamic anticancer treatment. *Nanomedicine* **2015**, *10*, 3483−3494.
(24) Huang, H.; Song, W.; Rieffel, J.; Lovell, J. F. Emerging applications of porphyrins in photomedicine. *Front. Phys.* **2015**, *3*, 1−23.
(25) Hammerer, F.; Garcia, G.; Chen, S.; Poyer, F.; Achelle, S.; Fiorini-debuisschert, C.; Maillard, P. Synthesis and characterization of glycoconjugated porphyrin triphenylamine hybrids for targeted two-photon photodynamic therapy. *J. Org. Chem.* **2014**, *79*, 1406−1417.
(26) Cheng, W.; Haedicke, I. E.; Nofiele, J.; Martinez, F.; Beera, K.; Scholl, T. J.; Zhang, X. A. Complementary strategies for developing Gd-free high-field T_1 MRI contrast agents based on Mn^{III} porphyrins. *J. Med. Chem.* **2014**, *57*, 516−520.
(27) Dong, X.; Chen, H.; Qin, J.; Wei, C.; Liang, J.; Liu, T.; Lv, F. Thermosensitive porphyrin-incorporated hydrogel with four-arm PEG-PCL copolymer (II): Doxorubicin loaded hydrogel as a dual fluorescent drug delivery system for simultaneous imaging tracking *in vivo*. *Drug Delivery* **2017**, *24*, 641−650.
(28) Stender, A. S.; Marchuk, K.; Liu, C.; Sander, S.; Meyer, M. W.; Smith, E. A.; Huang, B. Single cell optical imaging and spectroscopy. *Chem. Rev.* **2013**, *113*, 2469−2527.
(29) Ptaszynska, A. A.; Trytek, M.; Borsuk, G.; Buczek, K.; Rybicka-jasinska, K.; Gryko, D. Porphyrins inactivate Nosema spp. microsporidia. *Sci. Rep.* **2018**, *8*, 5523.
(30) Bajju, G. D.; Ashu; Ahmed, A.; Devi, G. Synthesis and bioactivity of oxovanadium(IV) tetra(4-methoxyphenyl)-porphyrinsalicylates. *BMC Chem.* **2019**, *13*, 15.
(31) Garcia-sampedroa, A.; Taberob, A.; Mahameda, I.; Acedo, P. Multimodal use of the porphyrin TMPyP: From cancer therapy to antimicrobial applications. *J. Porphyrins Phthalocyanines* **2019**, *23*, 11−27.
(32) Saha, T. K.; Yoshikawa, Y.; Yasui, H.; Sakura, H. Oxovanadium-(IV)−porphyrin complex as a potent insulin-mimetic. Treatment of experimental type 1 diabetic mice by the complex [*meso*-tetrakis(4-sulfonatophenyl)porphyrinato]oxovanadate(IV)(4-). *Bull. Chem. Soc. Jpn.* **2006**, *79*, 1191−1200.
(33) Saha, T. K.; Yoshikawa, Y.; Sakurai, H. Improvement of hyperglycaemia and metabolic syndromes in type 2 diabetic KKAy mice by oral treatment with [*meso*-tetrakis(4-sulfonatophenyl) porphyrinato]oxovanadium(IV)(4-) complex. *J. Pharm. Pharmacol.* **2010**, *59*, 437−444.
(34) Pervin, S.; Shaha, C. K.; Karmaker, S.; Saha, T. K. Conjugation of insulin-mimetic [*meso*-tetrakis(4-sulfonatophenyl)porphyrinato]-zinc(II) with chitosan in aqueous solution: kinetics, equilibrium and thermodynamics. *Polym. Bull.* **2021**, *78*, 4527−4550.
(35) Kumar, S.; e Silva, J. A.; Wani, M. Y.; Gil, J. M.; Sobral, A. J. F. N. Carbon dioxide capture and conversion by an environmentally friendly chitosan based *meso*-tetrakis(4-sulfonatophenyl) porphyrin. *Carbohydr. Polym.* **2017**, *175*, 575−583.
(36) Liao, B.; Liu, R.; Huang, Y. A supramolecular chiroptical switch based on chitosan and anionic porphyrin complex film. *Polym. J.* **2007**, *39*, 1071−1077.
(37) Synytsya, A.; Synytsya, A.; Blafkova, P.; Volka, K.; Kral, V. Interaction of meso-tetrakis(4-sulphonatophenyl)porphine with chitosan in aqueous solutions. *Spectrochim. Acta, Part A* **2007**, *66*, 225−235.
(38) Synytsya, A.; Synytsya, A.; Blafkova, P.; Ederova, J.; Spevacek, J.; Slepicka, P.; Kral, V.; Volka, K. pH-controlled self-assembling of *meso*-tetrakis(4-sulfonatophenyl)porphyrin-chitosan complexes. *Biomacromolecules* **2009**, *10*, 1067−1076.

https://doi.org/10.1021/acsomega.3c05804
ACS Omega 2023, 8, 41612−41623

(39) Venkatesan, J.; Jayakumar, R.; Mohandas, A.; Bhatnagar, I.; Kim, S. Antimicrobial activity of chitosan-carbon nanotube hydrogels. *Materials* **2014**, *7*, 3946−3955.
(40) Brijmohan, S. B.; Swier, S.; Weiss, R. A.; Shaw, M. T. Synthesis and characterization of cross-linked sulfonated polystyrene vanoparticles. *Ind. Eng. Chem. Res.* **2005**, *44*, 8039−8045.
(41) Tesolekile, N.; Ncapayi, V.; Obiyenwa, G. K.; Matoetoe, M.; Songca, S.; Oluwafemi, O. S. Synthesis of *meso*-tetra-(4-sulfonatophenyl)porphyrin ($TPPS_4$)−CuInS/ZnS quantum dots conjugate as an improved photosensitizer. *Int. J. Nanomed.* **2019**, *14*, 7065−7078.
(42) Saha, T. K.; Bhoumik, N. C.; Karmaker, S.; Ahmed, M. G.; Ichikawa, H.; Fukumori, Y. Adsorption characteristics of reactive black 5 from aqueous solution onto chitosan. *Clean: Soil Air, Water* **2011**, *39*, 984−993.
(43) Saha, T. K.; Karmaker, S.; Alam, M. F. Kinetics, mechanism and thermodynamics involved in sorption of meso-tetrakis(4-sulfonatophenyl)-porphyrin onto chitosan in aqueous medium. *J. Porphyrins Phthalocyanines* **2014**, *18*, 240−250.
(44) Chiou, M. S.; Li, H. Y. Adsorption behavior of reactive dye in aqueous solution on chemical cross-linked chitosan beads. *Chemosphere* **2003**, *50*, 1095−1105.
(45) Kumar, M. N. V. R. A review of chitin and chitosan applications. *React. Funct. Polym.* **2000**, *46*, 1−27.
(46) Lagergren, S. Zur Theorie der Sogenannten Adsorption Gelöster Stoffe. *K. Sven. Vetenskapsakad Handl.* **1898**, *24*, 1−39.
(47) Ho, Y. S.; Mckay, G. Pseudo-second order model for sorption processes. *Process Biochem.* **1999**, *34*, 451−465.
(48) Elovich, S. Y.; Larinov, O. G. Theory of adsorption from solutions of nonelectrolytes on solid (I) equation adsorption from solutions and the analysis of its simplest form, (II) verification of the equation of adsorption isotherm from solutions. *Izv. Akad. Nauk. SSSR, Otd. Khim. Nauk.* **1962**, *2*, 209−216.
(49) Jabar, J. M.; Odusote, Y. A.; Alabi, K. A.; Ahmed, I. B. Kinetics and mechanisms of congo-red dye removal from aqueous solution using activated *Moringa oleifera* seed coat as adsorbent. *Appl. Water Sci.* **2020**, *10*, 136.
(50) López-luna, J.; Ramírez-montes, L. E.; Martinez-vargas, S.; Martínez, A. I.; Mijangos-ricardez, O. F.; González-chávez, M. C. A.; Carrillo-gonzález, R.; Solís-domínguez, F. A.; Cuevas-díaz, M. C.; Vázquez-hipólito, V. Linear and nonlinear kinetic and isotherm adsorption models for arsenic removal by manganese ferrite nanoparticles. *SN Appl. Sci.* **2019**, *1*, 950.
(51) Tejada-tovar, C.; Villabona-ortíz, A.; Gonzalez-delgado, A. D. Adsorption of azo-anionic dyes in a solution using modified coconut (*Cocos nucifera*) mesocarp: Kinetic and equilibrium study. *Water* **2021**, *13*, 1382.
(52) Marques, B. S.; Frantz, T. S.; Sant'Anna Cadaval Junior, T. R.; De almeida pinto, L. A.; Dotto, G. L. Adsorption of a textile dye onto piaçava fibers: Kinetic, equilibrium, thermodynamics, and application in simulated effluents. *Environ. Sci. Pollut. Res.* **2019**, *26*, 28584−28592.
(53) Onal, Y.; Basar, C. A.; Ozdemir, C. S. Investigation kinetics mechanisms of adsorption malachite green onto activated carbon. *J. Hazard. Mater.* **2007**, *146*, 194−203.
(54) Weber, W. J., Jr; Morris, J. C. Kinetics of adsorption on carbon from solution. *J. Sanit. Eng. Div. Proc. Am. Soc. Civil. Eng.* **1963**, *89*, 31−59.
(55) Pan, M.; Lin, X.; Xie, J.; Huang, X. Kinetic, equilibrium and thermodynamic studies for phosphate adsorption on aluminum hydroxide modified polygorskite nano-composites. *RSC Adv.* **2017**, *7*, 4492−4500.
(56) Cheng, C.; Deng, J.; Lei, B.; He, A.; Zhang, X.; Ma, L.; Li, S.; Zhao, C. Toward 3D grapheme oxide gels based adsorbents for high-efficient water treatment via the promotion of biopolymers. *J. Hazard. Mater.* **2013**, *263*, 467−478.
(57) Freundlich, H. M. Over the adsorption in solutions. *Z. Phys. Chem.* **1906**, *57*, 385−470.
(58) Temkin, M. I.; Pyzhev, V. Kinetic of ammonia synthesis on promoted iron catalyst. *Acta Physicochim. URSS* **1940**, *12*, 327−356.
(59) Langmuir, I. The adsorption of gases on plane surfaces of glass, mica and platinum. *J. Am. Chem. Soc.* **1918**, *40*, 1361−1403.
(60) Udaybhaskar, P.; Iyengar, L.; Rao, A. V. S. P. Hexavalent chromium interaction with chitosan. *J. Appl. Polym. Sci.* **1990**, *39*, 739−747.
(61) Chan, L. S.; Cheung, W. H.; Allen, S. J.; Mckay, G. Error analysis of adsorption isotherm models for acid dyes onto bamboo derived activated carbon. *Chin. J. Chem. Eng.* **2012**, *20*, 535−542.
(62) Sadeq, N. M. Kinetics and thermodynamics of β-1 endosulfan pesticide adsorption in Jordan valley soils. *Glob. J. Sci. Front. Res. (B) Chemistry* **2018**, *18*, 250603.
(63) Petrolekas, P. D.; Maggenakis, G. Kinetic studies of the liquid-phase adsorption of a reactive dye onto activated lignite. *Ind. Eng. Chem. Res.* **2007**, *46*, 1326−1332.
(64) Liu, Y. Some consideration on the Langmuir isotherm equation. *Colloids Surf., A* **2006**, *274*, 34−36.
(65) Saha, P.; Chowdhury, S. Insight into adsorption thermodynamics. In *Thermodynamics*; Tadashi, M., Ed.; InTech.: Europe, 2011; pp 349−364.
(66) Imran, M.; Ramzan, M.; Qureshi, A. K.; Khan, M. A.; Tariq, M. Emerging applications of porphyrins and metalloporphyrins in biomedicine and diagnostic magnetic resonance imaging. *Biosensors* **2018**, *8*, 95.
(67) Chiou, M. S.; Li, H. Y. Adsorption behavior of reactive dye in aqueous solution on chemical crosslinked chitosan beads. *Chemosphere* **2003**, *50*, 1095−1105.
(68) Unagolla, J. M.; Jayasuriya, A. C. Drug transport mechanisms and in vitro release kinetics of vancomycin encapsulated chitosan-alginate polyelectrolyte microparticles as a controlled drug delivery system. *Eur. J. Pharm. Sci.* **2018**, *114*, 199−209.
(69) Liu, Y.; Sun, M.; Wang, T.; Chen, X.; Wang, H. Chitosan-based self-assembled nanomaterials: Their application in drug delivery. *View* **2020**, *2*, No. 20200069.

https://doi.org/10.1021/acsomega.3c05804
ACS Omega 2023, 8, 41612−41623